

Excitation-tailored dual-color emission of manganese(II)-doped perovskite nanocrystals ^{EP}

Cite as: Appl. Phys. Lett. **114**, 041902 (2019); <https://doi.org/10.1063/1.5081730>

Submitted: 15 November 2018 . Accepted: 13 January 2019 . Published Online: 30 January 2019

Zhangzhang Chen, Hongfei Chen, Chunfeng Zhang ^{id}, Lan Chen, Zhengyuan Qin, Hai Sang ^{id}, Xiaoyong Wang, and Min Xiao

COLLECTIONS

^{EP} This paper was selected as an Editor's Pick



View Online



Export Citation



CrossMark



Measure Ready
M91 FastHall™ Controller

A revolutionary new instrument
for complete Hall analysis

Lake Shore
CRYOTRONICS

Excitation-tailored dual-color emission of manganese(II)-doped perovskite nanocrystals

Cite as: Appl. Phys. Lett. **114**, 041902 (2019); doi: [10.1063/1.5081730](https://doi.org/10.1063/1.5081730)

Submitted: 15 November 2018 · Accepted: 13 January 2019 · Published Online: 30 January 2019




View Online



Export Citation



CrossMark

Zhangzhang Chen,¹ Hongfei Chen,¹ Chunfeng Zhang,^{1,a)}  Lan Chen,¹ Zhengyuan Qin,¹ Hai Sang,¹  Xiaoyong Wang,¹ and Min Xiao^{1,2}

AFFILIATIONS

¹ National Laboratory of Solid State Microstructures, School of Physics, Collaborative Innovation Center of Advanced Microstructures, Nanjing University, Nanjing 210093, China

² Department of Physics, University of Arkansas, Fayetteville, Arkansas 72701, USA

^{a)} E-mail: cfzhang@nju.edu.cn

ABSTRACT

Manganese(II)-doped perovskite nanocrystals with superior dual-color light emission properties are promising for optoelectronic applications. Here, we report that the emission color of these nanocrystals can be tailored by continuous-wave excitation because of the saturation of dopant emission at a record low light density (~ 10 mW/cm²). By detuning the repetition rates of excitation laser sources, we show that the bottleneck of exciton-manganese(II) energy transfer caused by the imbalanced excitation and deexcitation of ⁴T₁ states is the primary mechanism underlying the emission saturation properties. Such a dual-color luminescence tunable by weak excitation is promising for uses in potential applications such as luminescent solar concentrators, light intensity sensors, anti-counterfeit printing, and photo-switchable image markers.

Published under license by AIP Publishing. <https://doi.org/10.1063/1.5081730>

Nanocrystals (NCs) of lead halide perovskites have recently attracted great interest because of their favorable optoelectronic properties including strong light absorption, highly efficient photoluminescence (PL) emission, and color tunability through composition engineering.^{1–9} These features are pivotal for applying perovskite semiconductor NCs in color-selectable narrow-line-width light-emitting diodes (LEDs),^{10–14} low-threshold lasers,^{15–17} quantum light emitters,^{18–22} solar cells,^{23–26} photodetectors,²⁷ and radiation scintillators.^{28,29} Impurity doping can provide an additional level of control over the electronic, magnetic, and optical properties of semiconductor NCs.^{30–32} Doping perovskite NCs with manganese(II) (Mn²⁺) has been widely studied because such NCs display dual emission colors: the efficient yellow emission from the Mn²⁺ and the band-edge recombination in NCs.^{33–38} The dual-color emission from Mn²⁺-doped perovskite NCs makes them promising for use in high performance LEDs,^{39–41} luminescent solar concentrators,^{42,43} and biomedical imaging.⁴⁴

In Mn²⁺-doped NCs, the yellow luminescence from Mn²⁺ originates from the internal ⁴T₁ to ⁶A₁ transition, which is an electric-dipole forbidden process with an extremely long relaxation lifetime (τ_{Mn} of ~ 1 ms).^{45,46} The Mn²⁺ ions are excited by the

energy transfer from photo-induced excitons in the NCs occurring on the nanosecond time scale ($\tau_{ET} \sim 3$ –8 ns).^{33,34} The lifetimes of excitation and deexcitation processes are highly imbalanced ($\tau_{Mn} \gg \tau_{ET}$), leading to a bottleneck of energy transfer upon high density excitation.⁴⁶ Together with Auger recombination in semiconductor NCs⁴⁷ and nonradiative cross relaxation in Mn²⁺,⁴⁸ the energy-transfer bottleneck may substantially modify the intensity ratio between the band-edge emission and the dopant emission with changing excitation density. Such color-tunable luminescence has been intensively studied for Mn²⁺-doped chalcogenide II–VI semiconductor NCs^{46–49} but remains poorly understood for Mn²⁺-doped perovskite NCs.

Here, we report the tailoring of the dual-color emission from Mn²⁺-doped perovskite NCs with a continuous-wave (CW) laser at a record low light density and its underlying mechanism. Upon CW excitation, the PL from Mn²⁺ ions saturates at an excitation level of 10 mW/cm², which is over one-order of magnitude lower than that in Mn²⁺-doped chalcogenide II–VI semiconductor NCs. We unambiguously show that the primary mechanism is a bottleneck of exciton-Mn²⁺ energy transfer by conducting measurements with pulse excitations at different repetition rates. Such light-driven color-tunable emission may

be applied to high-power light sensors, anti-counterfeit printing, and photo-switchable image markers.

Samples of Mn^{2+} -doped CsPbCl_3 NCs are prepared by hot-injection synthesis, as described in the [supplementary material](#).^{3,33,34} The doping level of Mn^{2+} ions (x) is controlled by varying the feed molar ratio of MnCl_2 to PbCl_2 . The exact doping levels in each sample were characterized post-synthesis by inductively coupled plasma optical emission spectrometry (ICP-OES, Optima 5300DV). Transmission electron microscopy (TEM, TECNAI F20) and X-ray diffraction (XRD, Rigaku D/MAX-Ultima III) were used to characterize the morphology and the crystal structure of Mn^{2+} -doped CsPbCl_3 NCs. For optical measurements, toluene solutions of samples were added to a 1 mm-thick quartz cuvette with an optical density of ~ 0.3 at the lowest lying excitonic features. The PL spectra of the NCs were measured using a monochromator (Acton SP2500, Princeton Instruments) equipped with a liquid- N_2 cooled charge-coupled device (CCD; Spec-10 400BX, Princeton Instruments). For CW and pulsed excitations with repetition rates above 1 MHz, we used a laser diode at the wavelength of 375 nm (LDH-D-C-375, Picoquant) working in the CW and pulse modes. For excitations with repetition rates below 1 MHz, a picosecond optical parameter amplifier (Pico AOT MOPA, Innolas) was used at 355 nm. The excitation photon flux was calibrated for the two lasers. The decay lifetime of band-edge emission was measured by time-correlated single-photon counting (TCSPC, PicoHarp 300, Picoquant) under the 375 nm pulsed excitation with a repetition rate of 10 MHz. The lifetime of Mn^{2+} emission is much longer than the time intervals of the laser pulses for TCSPC, so we recorded the decay dynamics of Mn^{2+} emission using a photodetector (DET36A/M, Thorlabs) and an oscilloscope (DSO9254A, Agilent Technologies) under the 355 nm pulsed excitation with a repetition rate of 100 Hz. All the experiments were conducted at room temperature.

TEM analysis reveals that the $\text{CsMn}_x\text{Pb}_{1-x}\text{Cl}_3$ NCs [Fig. 1(a)] have similar morphologies to those of undoped samples (Fig. S1 in the [supplementary material](#)). XRD patterns [Fig. 1(b)] indicate that the samples with and without Mn^{2+} possessed identical structures. With the increasing doping level, a monotonical peak shift is observed, which can be ascribed to the lattice contraction caused by the replacement of the larger Pb^{2+} (133 pm) by the smaller Mn^{2+} (97 pm).³³ These results confirm the doping of Mn^{2+} in the perovskite NCs. The absorption and PL emission spectra [Figs. 1(c) and 1(d)] of $\text{CsMn}_x\text{Pb}_{1-x}\text{Cl}_3$ NCs strongly depend on the Mn^{2+} doping level. The absorption cross section at 375 nm is $\sim 5 \times 10^{-14} \text{ cm}^2$ in CsPbCl_3 NCs. With an increased doping level, a slight blue shift is observed in the absorption spectra due to the effect of Mn alloying on the bandgap of the NCs [Fig. 1(c)],^{33,50} which is also manifested in the spectra of band-edge emission [Fig. 1(d)]. The dopant emission centered at 600 nm is far from the absorption edge of the perovskite NCs, which is particularly suitable for applications in luminescent color concentrators.⁴³ In addition, the intensity ratio between the dopant emission and band-edge emission ($\eta = I_{\text{Mn}}/I_{\text{EX}}$) increases with the increasing doping level because of the enhanced energy transfer from the NCs to Mn^{2+} dopants [Fig. 1(d)].

Figure 2 shows the excitation-density-dependent PL spectra observed from a solution sample of $\text{CsMn}_x\text{Pb}_{1-x}\text{Cl}_3$ NCs

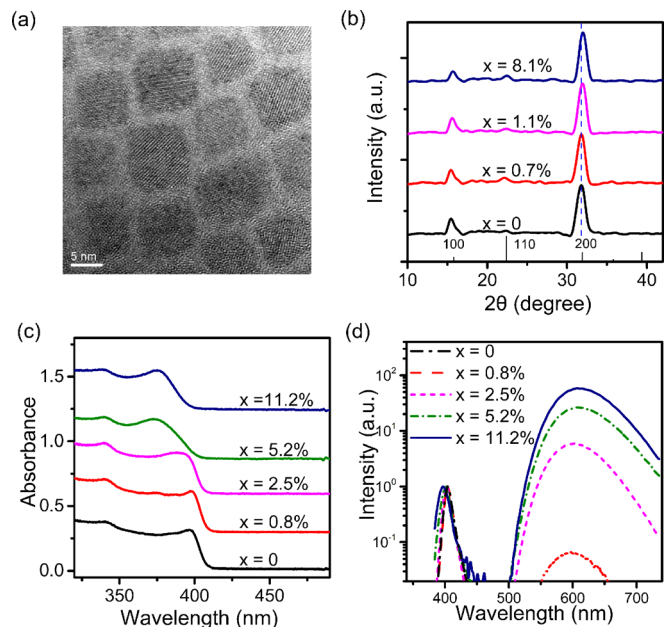


FIG. 1. (a) Typical TEM images of $\text{CsMn}_x\text{Pb}_{1-x}\text{Cl}_3$ NCs ($x = 11.2\%$). (b) XRD patterns, (c) absorption, and (d) PL spectra of the solution samples of Mn^{2+} -doped CsPbCl_3 NCs with different doping levels (x). The PL spectra are plotted on a scale normalized to the band-edge emission.

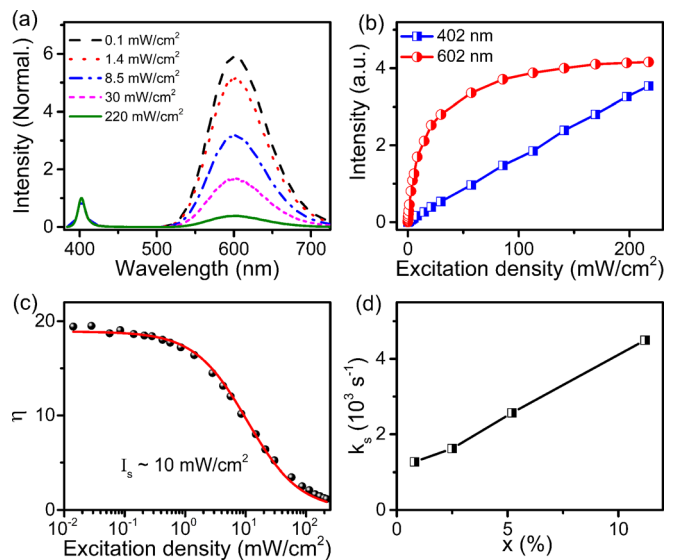


FIG. 2. (a) PL spectra recorded for $\text{CsMn}_x\text{Pb}_{1-x}\text{Cl}_3$ NCs ($x = 2.5\%$) under CW excitation at different densities. The spectra are plotted on a scale normalized to the band-edge emission. (b) Integrated intensities of the Mn^{2+} emission band centered at 602 nm and the band-edge emission band centered at 402 nm are plotted against excitation density. (c) The intensity ratio of the Mn^{2+} emission to the band-edge emission (η) is plotted against excitation density. The solid line is the fitting curve using Eq. (1) with the saturation excitation density of $I_s \sim 10 \text{ mW/cm}^2$. (d) Saturation excitation rate (k_s) in $\text{CsMn}_x\text{Pb}_{1-x}\text{Cl}_3$ NCs is plotted versus the doping level.

($x = 0.025$) under a CW laser irradiation. The normalized spectral profiles [Fig. 2(a)] indicate that η gradually decreases with increasing excitation density. Such an excitation-density-dependent PL spectral profile is mainly induced by the saturation behavior of Mn^{2+} emission [Fig. 2(b)]. As illustrated in Fig. 2(b), the intensity of band-edge emission is linearly dependent on the excitation density in the considered range, but the dopant emission shows a sublinear dependence on the excitation density and saturates at high excitation density. To quantify the excitation density dependence, we analyze the intensity ratio (η) between the yellow emission and band-edge emission with a phenomenological model of

$$\eta(I) = \frac{\eta_0}{1 + I/I_s}, \quad (1)$$

where η_0 is a constant describing the intensity ratio at the weak excitation limit, I is the excitation density, and I_s is the saturation excitation density. The model can well reproduce the measured dependence of $\eta(I)$ on the excitation density [Fig. 2(c)] with a saturation excitation density of $I_s \sim 10 \text{ mW/cm}^2$. This value is over one-order of magnitude weaker than that estimated in Mn^{2+} -

doped II-VI chalcogenide NCs (Fig. S3 in the supplementary material). Such a significant difference is related to the stronger light-matter interaction in perovskite NCs than that in conventional II-VI semiconductor NCs which is manifested with about one-order of magnitude increase in the absorption cross section.¹ To compare the saturation effect in different samples, we use the saturation excitation rate (k_s) defined as $k_s = \sigma I_s/h\nu$, where σ is the absorption cross section and $h\nu$ is the excitation photon energy at the incident wavelength. The k_s value of Mn^{2+} -doped perovskite NCs [Fig. 2(d)] is of the order of 10^3 s^{-1} , which is comparable to those obtained in conventional II-VI chalcogenide NCs (Fig. S3 in the supplementary material). With the increasing doping level, k_s increases monotonically because of the increased density of available ${}^4\text{T}_1$ states [Fig. 2(d)].

Several mechanisms have been proposed to explain the saturation of dopant emission in conventional Mn^{2+} -doped II-VI semiconductor NCs.^{46–49} Besides the initially proposed bottleneck effect for energy transfer from excitons to ${}^4\text{T}_1$ states in dopants [Fig. 3(a)],⁴⁶ different types of many-body effects such as multiexciton Auger recombination in NCs [Fig. 3(b)],⁴⁷ consecutive exciton- Mn^{2+} energy transfer [Fig. 3(c)],⁴⁹ and

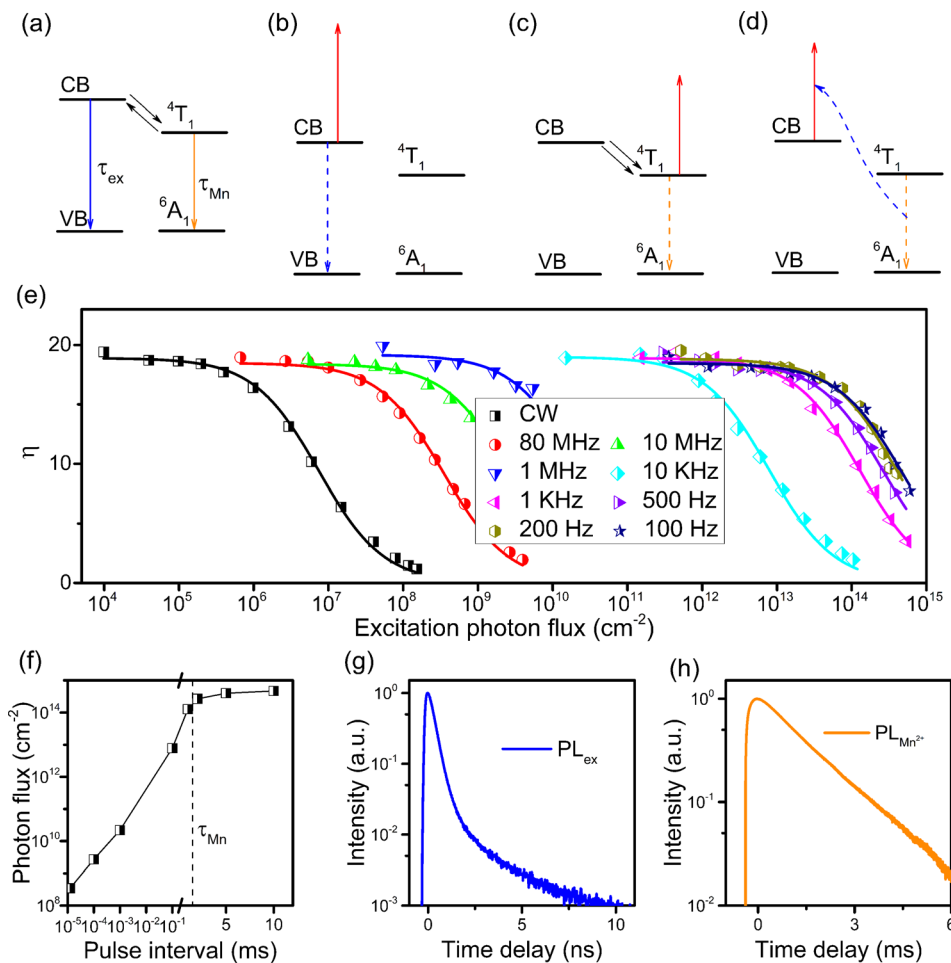


FIG. 3. Schematic diagrams of the processes of (a) energy transfer and radiative emissions in Mn^{2+} -doped perovskite NCs, (b) Auger process in perovskite NCs, (c) consecutive exciton- Mn^{2+} energy transfer, and (d) exciton- Mn^{2+} cross relaxation. (e) The intensity ratio of the Mn^{2+} emission to the band-edge emission (η) from $\text{CsMn}_x\text{Pb}_{1-x}\text{Cl}_3$ NCs ($x = 2.5\%$) plotted against excitation photon flux under CW and pulsed excitations at different repetition rates. For pulse excitation, the excitation photon flux is calculated as the number of incident photons per pulse per cm^2 . For CW excitation, the excitation photon flux is calculated as the number of incident photons per cm^2 within the PL lifetime of perovskite NCs. (f) Saturation photon flux plotted against the pulse interval. The dashed line indicates the lifetime of Mn^{2+} emission. PL decay dynamics of (g) band-edge emission and (h) Mn^{2+} emission.

Mn^{2+} -exciton cross relaxation [Fig. 3(d)]⁴⁸ processes have been reported. To uncover the central mechanism governing the saturation of dopant emission in Mn^{2+} -doped perovskite NCs, we perform the measurements with pulsed lasers at different repetition rates [Fig. 3(e)]. The excitation photon flux is used to compare the excitation densities at different repetition rates. The saturation excitation photon flux is highly sensitive to the repetition rate [Figs. 3(e) and 3(f)]. In Fig. 3(f), we plot the saturation photon flux as a function of the time interval between excitation pulses. When the time interval is shorter than τ_{Mn} ,⁴⁵ the saturation photon flux dramatically increases with an extending time interval. The population accumulation effect is crucial here, which can be regarded as an evidence of the depletion of population at the $^4\text{T}_1$ states upon high-density excitation. As shown in Fig. 3(a), the $^4\text{T}_1$ states are excited by impact excitation from photo-excited excitons in the perovskite NCs. Such an energy transfer process is only efficient when its rate is comparable to that of the interband recombination in semiconductor NCs. Since the decay lifetime of band-edge emission is ~ 0.4 ns [Fig. 3(g)], the characterized lifetime of an efficient energy transfer process should be on the timescale of nanoseconds or shorter, which is consistent with the value estimated in the literature.³³ However, the deexcitation process of $^4\text{T}_1$ states in the sample is extremely slow [~ 1.5 ms, Fig. 3(h)]. When the time interval is shorter than the deexcitation, the population accumulation at $^4\text{T}_1$ states will set a bottleneck that limits the energy transfer when excitation density increases. Because of the long lifetime of $^4\text{T}_1$ states, the consecutive exciton- Mn^{2+} energy transfer [Fig. 3(c)]⁴⁹ and Mn^{2+} -exciton cross relaxation [Fig. 3(d)]⁴⁸ processes may be triggered. In consequence, PL emission from the dopants is strongly suppressed at high excitation density. When the time interval is much longer than τ_{Mn} , the accumulation effect plays an unimportant role. Instead, multiexciton Auger recombination [Fig. 3(b)]⁴⁷ becomes the primary cause of the saturation effect. From the above results, we conclude that the saturation effect under CW weak excitation is mainly caused by the bottleneck limiting energy transfer from excitons to dopants.

From the perspective of applications, the saturation of light emission upon weak excitation may hinder the practical operation of the LEDs using Mn^{2+} -doped perovskite NCs in high-brightness lightening. Such a side effect may be suppressed by increasing the doping level. The excitation-tailored color tunability of the NCs also shows great potential for many applications. To demonstrate the excitation-controlled emission color of these nanocrystals, we extend the bandgap of the perovskite NCs to the blue range by introducing Br in the NCs. Figure 4(a) shows the absorption spectrum of a solution of Br-doped NCs through post-synthetic halide exchange. Br doping tunes the band-edge emission to ~ 450 nm. In such a sample of $\text{CsMn}_x\text{Pb}_{1-x}\text{Cl}_{3-y}\text{Br}_y$, PL emission contains a mixture of the blue and yellow bands, the intensity ratio of which can be controlled by the excitation density [Fig. 4(b)]. The emission colors of the NCs under different CW excitations are marked in the International Commission on Illumination (CIE) 1931 color space chromaticity diagram in Fig. 4(c). The emission color changes from nearly orange to pink and finally to purple-blue with increasing excitation density. Once calibrated in quantity, the intensity ratio can be used as a metric

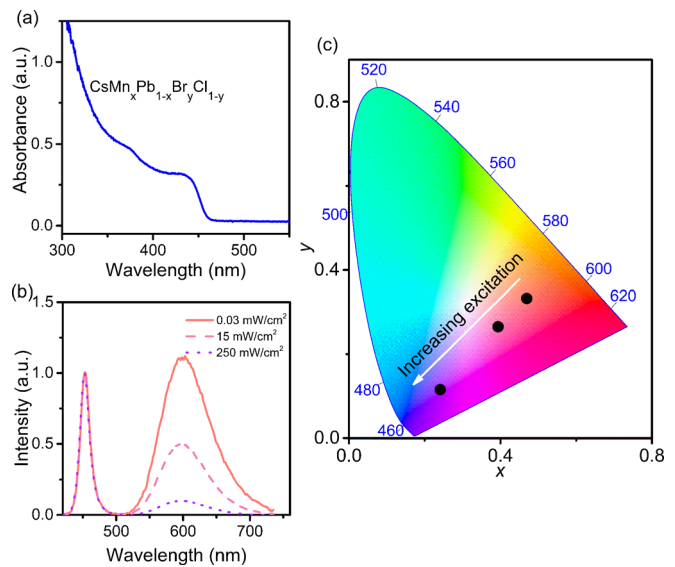


FIG. 4. (a) Absorption spectrum of a solution sample of $\text{CsMn}_x\text{Pb}_{1-x}\text{Br}_y\text{Cl}_{3-y}$ NCs and (b) normalized PL spectra for the sample under CW excitation of 0.03, 15, and 250 W/cm^2 . (c) Excitation-density-dependent emission colors of the sample are shown in the CIE color space chromaticity diagram.

for light intensity sensing. These color changes are fully reversible, which is beneficial for practical applications.

In summary, we have demonstrated the saturation of dopant emission in Mn^{2+} -doped perovskite NCs at a marked low excitation density. Such a saturation effect enables the control of dual-color emission at a marked low excitation density benefiting from the strong light-matter interaction in perovskite NCs. We present compelling evidence to show that this effect is primarily induced by the bottleneck of exciton- Mn^{2+} energy transfer resulting from the long-lived population at the $^4\text{T}_1$ states in the dopant ions. The excitation-controlled color-tunable emission displayed by these NCs should aid the design and synthesis of functional nanomaterials. Color tunability realized upon weak CW excitation is of great promise for uses in light sensors, luminescent solar concentrators, anti-counterfeit printing, and photo-switchable image markers.

See [supplementary material](#) for sample preparation details, TEM characterization of CsPbCl_3 NCs (Fig. S1), excitation-dependent dual-color emission in Mn^{2+} -doped CsPbBr_3 NCs with different doping levels (Fig. S2), and Mn^{2+} -doped II-VI semiconductor NCs (Fig. S3).

This work was supported by the National Key R&D Program of China (2018YFA0209100 and 2017YFA0303703), the National Natural Science Foundation of China (21873047, 11574140, 91850105, 91833305, and 11621091), Jiangsu Provincial Funds for Distinguished Young Scientists (BK20160019), the Priority Academic Program Development of Jiangsu Higher Education Institutions (PAPD), and the Fundamental Research Funds for the Central Universities. C.Z. acknowledges the

financial support from the Tang Scholar program. The authors acknowledge Dr. Xuewei Wu for his technical assistance.

REFERENCES

- ¹Q. A. Akkerman, G. Raino, M. V. Kovalenko, and L. Manna, *Nat. Mater.* **17**, 394 (2018).
- ²M. V. Kovalenko, L. Protesescu, and M. I. Bodnarchuk, *Science* **358**, 745 (2017).
- ³L. Protesescu, S. Yakunin, M. I. Bodnarchuk, F. Krieg, R. Caputo, C. H. Hendon, R. X. Yang, A. Walsh, and M. V. Kovalenko, *Nano Lett.* **15**, 3692 (2015).
- ⁴F. Zhang, H. Zhong, C. Chen, X.-g. Wu, X. Hu, H. Huang, J. Han, B. Zou, and Y. Dong, *ACS Nano* **9**, 4533 (2015).
- ⁵Q. A. Akkerman, V. D'Innocenzo, S. Accornero, A. Scarpellini, A. Petrozza, M. Prato, and L. Manna, *J. Am. Chem. Soc.* **137**, 10276 (2015).
- ⁶Y. Bekenstein, B. A. Koscher, S. W. Eaton, P. Yang, and A. P. Alivisatos, *J. Am. Chem. Soc.* **137**, 16008 (2015).
- ⁷A. Swarnkar, R. Chulliyil, V. K. Ravi, M. Irfanullah, A. Chowdhury, and A. Nag, *Angew. Chem. Int. Ed.* **54**, 15424 (2015).
- ⁸Y. Tong, E. Bladt, M. F. Ayguler, A. Manzi, K. Z. Milowska, V. A. Hintermayr, P. Docampo, S. Bals, A. S. Urban, L. Polavarapu, and J. Feldmann, *Angew. Chem. Int. Ed.* **55**, 13887 (2016).
- ⁹X. Zhang, X. Bai, H. Wu, X. Zhang, C. Sun, Y. Zhang, W. Zhang, W. Zheng, W. W. Yu, and A. L. Rogach, *Angew. Chem. Int. Ed.* **57**, 3337 (2018).
- ¹⁰J. Song, J. Li, X. Li, L. Xu, Y. Dong, and H. Zeng, *Adv. Mater.* **27**, 7162 (2015).
- ¹¹L. Xiaoming, W. Ye, Z. Shengli, C. Bo, G. Yu, S. Jizhong, and H. Zeng, *Adv. Funct. Mater.* **26**, 2435 (2016).
- ¹²M. Yuan, L. N. Quan, R. Comin, G. Walters, R. Sabatini, O. Voznyy, S. Hoogland, Y. Zhao, E. M. Bearegard, P. Kanjanaboos, Z. Lu, D. H. Kim, and E. H. Sargent, *Nat. Nanotechnol.* **11**, 872 (2016).
- ¹³X. Zhang, H. Lin, H. Huang, C. Reckmeier, Y. Zhang, W. C. Choy, and A. L. Rogach, *Nano Lett.* **16**, 1415 (2016).
- ¹⁴G. Li, F. W. Rivarola, N. J. Davis, S. Bai, T. C. Jellicoe, F. de la Pena, S. Hou, C. Ducati, F. Gao, R. H. Friend, N. C. Greenham, and Z. K. Tan, *Adv. Mater.* **28**, 3528 (2016).
- ¹⁵Y. Wang, X. Li, J. Song, L. Xiao, H. Zeng, and H. Sun, *Adv. Mater.* **27**, 7101 (2015).
- ¹⁶S. Yakunin, L. Protesescu, F. Krieg, M. I. Bodnarchuk, G. Nedelcu, M. Humer, G. D. Luca, M. Fiebig, W. Heiss, and M. V. Kovalenko, *Nat. Commun.* **6**, 8056 (2015).
- ¹⁷Y. Xu, Q. Chen, C. Zhang, R. Wang, H. Wu, X. Zhang, G. Xing, W. W. Yu, X. Wang, Y. Zhang, and M. Xiao, *J. Am. Chem. Soc.* **138**, 3761 (2016).
- ¹⁸C. Yin, L. Chen, N. Song, Y. Lv, F. Hu, C. Sun, W. W. Yu, C. Zhang, X. Wang, Y. Zhang, and M. Xiao, *Phys. Rev. Lett.* **119**, 026401 (2017).
- ¹⁹F. Hu, H. Zhang, C. Sun, C. Yin, B. Lv, C. Zhang, W. W. Yu, X. Wang, Y. Zhang, and M. Xiao, *ACS Nano* **9**, 12410 (2015).
- ²⁰Y.-S. Park, S. Guo, N. S. Makarov, and V. I. Klimov, *ACS Nano* **9**, 10386 (2015).
- ²¹M. Fu, P. Tamarat, H. Huang, J. Even, A. L. Rogach, and B. Lounis, *Nano Lett.* **17**, 2895 (2017).
- ²²J. Ramade, L. M. Andriambarijaona, V. Steinmetz, N. Goubet, L. Legrand, T. Barisien, F. Bernardot, C. Testelin, E. Lhuillier, A. Bramati, and M. Chamarro, *Appl. Phys. Lett.* **112**, 072104 (2018).
- ²³A. Swarnkar, A. R. Marshall, E. M. Sanehira, B. D. Chernomordik, D. T. Moore, J. A. Christians, T. Chakrabarti, and J. M. Luther, *Science* **354**, 92 (2016).
- ²⁴E. M. Sanehira, A. R. Marshall, J. A. Christians, S. P. Harvey, P. N. Ciesielski, L. M. Wheeler, P. Schulz, L. Y. Lin, M. C. Beard, and J. M. Luther, *Sci. Adv.* **3**, eaao4204 (2017).
- ²⁵T. Zhang, M. Ibrahim Dar, L. Ge, X. Feng, N. Guo, M. Grätzel, and Y. Zhao, *Sci. Adv.* **3**, 1700841 (2017).
- ²⁶J. Xue, J.-W. Lee, Z. Dai, R. Wang, S. Nuryyeva, M. E. Liao, S.-Y. Chang, L. Meng, D. Meng, P. Sun, O. Lin, M. S. Goorsky, and Y. Yang, *Joule* **2**, 1866 (2018).
- ²⁷P. Ramasamy, D. H. Lim, B. Kim, S. H. Lee, M. S. Lee, and J. S. Lee, *Chem. Commun.* **52**, 2067 (2016).
- ²⁸Q. Chen, J. Wu, X. Ou, B. Huang, J. Almutlaq, A. A. Zhumekenov, X. Guan, S. Han, L. Liang, Z. Yi, J. Li, X. Xie, Y. Wang, Y. Li, D. Fan, D. B. L. Teh, A. H. All, O. F. Mohammed, O. M. Bakr, T. Wu, M. Bettinelli, H. Yang, W. Huang, and X. Liu, *Nature* **561**, 88 (2018).
- ²⁹J. H. Heo, D. H. Shin, J. K. Park, D. H. Kim, S. J. Lee, and S. H. Im, *Adv. Mater.* **30**, 1801743 (2018).
- ³⁰D. J. Norris, A. L. Efros, and S. C. Erwin, *Science* **319**, 1776 (2008).
- ³¹R. Beaulac, L. Schneider, P. I. Archer, G. Bacher, and D. R. Gamelin, *Science* **325**, 973 (2009).
- ³²T. He, J. Li, C. Ren, S. Xiao, Y. Li, R. Chen, and X. Lin, *Appl. Phys. Lett.* **111**, 211105 (2017).
- ³³W. Liu, Q. Lin, H. Li, K. Wu, I. Robel, J. M. Pietryga, and V. I. Klimov, *J. Am. Chem. Soc.* **138**, 14954 (2016).
- ³⁴D. Parobek, B. J. Roman, Y. Dong, H. Jin, E. Lee, M. Sheldon, and D. H. Son, *Nano Lett.* **16**, 7376 (2016).
- ³⁵S. Das Adhikari, S. K. Dutta, A. Dutta, A. K. Guria, and N. Pradhan, *Angew. Chem. Int. Ed.* **56**, 8746 (2017).
- ³⁶C. C. Lin, K. Y. Xu, D. Wang, and A. Meijerink, *Sci. Rep.* **7**, 45906 (2017).
- ³⁷J. Zhu, X. Yang, Y. Zhu, Y. Wang, J. Cai, J. Shen, L. Sun, and C. Li, *J. Phys. Chem. Lett.* **8**, 4167 (2017).
- ³⁸K. Xu and A. Meijerink, *Chem. Mater.* **30**, 5346 (2018).
- ³⁹H. Liu, Z. Wu, J. Shao, D. Yao, H. Gao, Y. Liu, W. Yu, H. Zhang, and B. Yang, *ACS Nano* **11**, 2239 (2017).
- ⁴⁰S. Zou, Y. Liu, J. Li, C. Liu, R. Feng, F. Jiang, Y. Li, J. Song, H. Zeng, M. Hong, and X. Chen, *J. Am. Chem. Soc.* **139**, 11443 (2017).
- ⁴¹Q. Wei, M. Li, Z. Zhang, J. Guo, G. Xing, T. C. Sum, and W. Huang, *Nano Energy* **51**, 704 (2018).
- ⁴²Q. Wang, X. Zhang, Z. Jin, J. Zhang, Z. Gao, Y. Li, and S. F. Liu, *ACS Energy Lett.* **2**, 1479 (2017).
- ⁴³F. Meinardi, Q. A. Akkerman, F. Bruni, S. Park, M. Mauri, Z. Dang, L. Manna, and S. Brovelli, *ACS Energy Lett.* **2**, 2368 (2017).
- ⁴⁴J. H. Yu, S.-H. Kwon, Z. Petrasek, O. K. Park, S. W. Jun, K. Shin, M. Choi, Y. I. Park, K. Park, H. B. Na, N. Lee, D. W. Lee, J. H. Kim, P. Schwillie, and T. Hyeon, *Nat. Mater.* **12**, 359 (2013).
- ⁴⁵C. Gan, Y. Zhang, D. Battaglia, X. Peng, and M. Xiao, *Appl. Phys. Lett.* **92**, 241111 (2008).
- ⁴⁶O. Chen, D. E. Shelby, Y. Yang, J. Zhuang, T. Wang, C. Niu, N. Omenetto, and Y. C. Cao, *Angew. Chem. Int. Ed.* **49**, 10132 (2010).
- ⁴⁷S. Taguchi, A. Ishizumi, and Y. Kanemitsu, *J. Phys. Soc. Jpn.* **79**, 063710 (2010).
- ⁴⁸L. R. Bradshaw, A. Hauser, E. J. McLaurin, and D. R. Gamelin, *J. Phys. Chem. C* **116**, 9300 (2012).
- ⁴⁹H.-Y. Chen, T.-Y. Chen, E. Berdugo, Y. Park, K. Lovering, and D. H. Son, *J. Phys. Chem. C* **115**, 11407 (2011).
- ⁵⁰V. A. Vlaskin, C. J. Barrows, C. S. Erickson, and D. R. Gamelin, *J. Am. Chem. Soc.* **135**, 14380 (2013).